ANL-ARC-195

Development and Validation of a Radial Inflow Turbine Model for Simulation of the SNL S-CO_2 Split-Flow Loop

Nuclear Engineering Division

About Argonne National Laboratory

Argonne is a U.S. Department of Energy laboratory managed by UChicago Argonne, LLC under contract DE-AC02-06CH11357. The Laboratory's main facility is outside Chicago, at 9700 South Cass Avenue, Argonne, Illinois 60439. For information about Argonne, see http://www.anl.gov.

Availability of This Report

This report is available, at no cost, at http://www.osti.gov/bridge. It is also available on paper to the U.S. Department of Energy and its contractors, for a processing fee, from:

U.S. Department of Energy
Office of Scientific and Technical Information
P.O. Box 62
Oak Ridge, TN 37831-0062
phone (865) 576-8401
fax (865) 576-5728
reports@adonis.osti.gov

Disclaimer

This report was prepared as an account of work sponsored by an agency of the United States Government. Neither the United States Government nor any agency thereof, nor UChicago Argonne, LLC, nor any of their employees or officers, makes any warranty, express or implied, or assumes any legal liability or responsibility for the accuracy, completeness, or usefulness of any information, apparatus, product, or process disclosed, or represents that its use would not infringe privately owned rights. Reference herein to any specific commercial product, process, or service by trade name, trademark, manufacturer, or otherwise, does not necessarily constitute or imply its endorsement, recommendation, or favoring by the United States Government or any agency thereof. The views and opinions of document authors expressed herein do not necessarily state or reflect those of the United States Government or any agency thereof, Argonne National Laboratory, or UChicago Argonne, LLC.

ANL-ARC-195

Development and Validation of a Radial Inflow Turbine Model for Simulation of the SNL S-CO_2 Split-Flow Loop

Richard B. Vilim
Nuclear Engineering Division
Argonne National Laboratory

August 15, 2011

ABSTRACT

A one-dimensional model for a radial inflow turbine has been developed for super-critical carbon dioxide (S-CO_2) Brayton cycle applications. The model accounts for the main phenomena present in the volute, nozzle, and impeller of a single-stage turbine. These phenomena include internal losses due to friction, blade loading, and angle of incidence and parasitic losses due to windage and blade-housing leakage. The model has been added as a component to the G-PASS plant systems code.

The model was developed to support the analysis of S-CO_2 cycles in conjunction with small-scale loop experiments. Such loops operate at less than a MWt thermal input. Their size permits components to be reconfigured in new arrangements relatively easily and economically. However, the small thermal input combined with the properties of carbon dioxide lead to turbomachines with impeller diameters of only one to two inches. At these sizes the dominant phenomena differ from those in larger more typical machines. There is almost no treatment in the literature of turbomachines at these sizes. The present work therefore is aimed at developing turbomachine models that support the task of S-CO_2 cycle analysis using small-scale tests.

Model predictions were compared against data from an experiment performed for Sandia National Laboratories in the split-flow Brayton cycle loop currently located at Barber-Nichols Inc. The split-flow loop incorporates two turbo-alternator-compressor (TAC) units each incorporating a radial inflow turbine and a radial flow compressor on a common shaft. The predicted thermodynamic conditions at the outlet of the turbine on the main compressor shaft were compared with measured values at different shaft speeds. Two modifications to the original model were needed to better match the experiment data. First, a representation of the heat loss from the volute downstream of the sensed inlet temperature was added. Second, an empirical multiplicative factor was applied to the Euler head and another to the head loss to bring the predicted outlet pressure into better agreement with the experiment. These changes also brought the overall efficiency of the turbine into agreement with values cited by Barber Nichols for small turbines.

More generally, the quality of measurement set data can in the future be improved by additional steps taken in the design and operation of the experimental apparatus. First, a thermocouple mounted at the nozzle inlet would provide a better indication of temperature at this key point. Second, heat losses from the turbine should be measured directly. Allowing the impeller to free wheel at inlet conditions and measuring

the temperature drop between inlet and outlet would provide a more accurate measure of heat loss. Finally, the enthalpy change during operation is more accurately obtained by measuring the torque on the stator using strain gauges rather than by measuring pressure and temperature at inlet and outlet to infer thermodynamic states.

Table of Contents

ABSTRACT 5
List of Figures 9
List of Tables 9
1 Introduction 13
2 Turbine Model 13
2.1 Volute 15
2.2 Nozzle 17
2.2.1 Exit Velocity Angle 17
2.2.2 Incidence Loss 18
2.2.3 Form Loss 20
2.3 Impeller 20
2.3.1 Head 20
2.3.2 Incidence Loss 21
2.3.3 Channel-Flow Friction Loss 23
2.3.4 Blade-Loading Loss 24
2.3.5 Blade-Leakage Loss 24
2.3.6 Efficiency 26
2.4 Outlet 27
2.5 Parasitic Losses 27
2.5.1 Windage 27
2.6 Solution Algorithm 28
2.6.1 Volute 28
2.6.2 Nozzle 30
2.6.3 Impeller 32
3 Validation 35
3.1 Instrumentation 38
3.2 Sensitivity and Uncertainty Analysis 39
3.3 Volute Heat Loss 40
3.4 Comparison of Model with Data 42
4 Summary and Recommendations 45
5 References 46
APPENDIX Theoretical Impeller Head 48

LIST OF FIGURES

Figure 1.1 Radial Turbine Components and Stations 14
Figure 2.1 Dimension Variables for Volute 15
Figure 2.2 Schematic of Nozzle Geometric Parameters 18
Figure 2.3 View of Blade at Nozzle Inlet 19
Figure 2.4 Nozzle Inlet Velocity Triangles 19
Figure 2.5 Impeller Velocity Triangles 24
Figure 3.1 Simple Split-Flow Recuperated Brayton Cycle Layout of Test 101201-1041 36

LIST OF TABLES

Table 3.1 Turbine-Alternator-Compressor (TAC) Shafts and Associated Turbomachine Identities 36
Table 3.2 Volute Geometry Parameters for Turbine T-2 for Main Compressor 36
Table 3.3 Nozzle Geometry Parameters for Turbine T-2 for Main Compressor 37
Table 3.4 Impeller Geometry Parameters for Turbine T-2 for Main Compressor 38
Table 3.5 Sensitivity of Turbine Validation Quantities to Measurement Error 39
Table 3.6 Parameter Values for Volute Heat Loss Model at 25 kRPM 39
Table 3.7 Comparison of Turbine Model with Experiment Data 42
Table 3.8 Corrected Inlet Temperature and Enthalpy Measurements after Modeling Heat Loss through Volute Wall 43
Table 3.9 Turbine Model with Corrected Experiment Inlet Temperature and 0.85 Multiplicative Head Factor 43
Table 3.10 Turbine Model with Corrected Experiment Inlet Temperature, 0.85 Multiplicative Head Factor, and 0.5 Multiplicative Pressure Loss Factor 44
Table 3.11 Comparison of Turbine Model State Points against those Derived from Barber-Nichols Model 45

Nomenclature

P static pressure
c chord
H total specific enthalpy change
u internal energy
ρ density
σ slip factor
V absolute velocity
U tangential velocity
W relative velocity
H specific enthalpy; specific loss
n number of blades
r radius
s blade pitch, gap between blade and housing
b blade height
L channel length
w width
$\dot{m}$ mass flow rate
α angle between fluid and wheel tangent
β angle between blade and wheel tangent
Δ angle at inlet between blade and plane containing impeller eye
λ void fraction
γ angle between streamline and plane normal to impeller axis of rotation
μ viscosity
$\dot{\Omega}$ angular velocity
Φ angle at outlet between streamline and plane normal to axis of rotation
η efficiency
T torque
f friction factor, equation of state
D_h hydraulic diameter
Re Reynolds number
A unprojected area
D diameter
$\dot{Q}$ power imparted to the fluid in the control volume

Subscripts

i inlet, inner
o outlet, outer
t total
s static, short
b blade height, blade
cl clearance
f friction

1 outlet from impeller
2 inlet to impeller
3 outlet from nozzle
4 inlet to nozzle
5 volute
I impeller
N nozzle
inc incidence
bl blade loading
th throat
θ tangential component of velocity
r radial of velocity

1 Introduction

The single-stage radial inflow turbine has applicability to energy conversion cycles across a range of shaft powers. In the Sandia National Laboratory S-CO_2 test loop a single-stage radial turbine with an impeller diameter of 0.068 m can generate up to 30 KW of shaft power. If the blade diameter and height are each scaled by a factor 30, then the resulting 2 m diameter impeller generates 26 MWt of shaft power, based on a simple scaling using Euler's equation. While the relative importance of the different loss mechanisms varies significantly between these two cases, the result indicates the power levels that are achievable using a single stage.

This report describes a one-dimensional model for a single-stage radial turbine developed for use in the G-PASS code. Multiple stage radial turbines can be represented by concatenating single stages in series by the user through the code input. The radial turbine has its analog in the centrifugal compressor. The G-PASS centrifugal compressor model is described in [1].

2 Turbine Model

The model developed for the main turbine is based on the one-dimensional energy equation. The phenomena are represented as source and loss terms and are summed to provide the overall enthalpy change and the shaft work, both as a function of mass flow rate and angular speed. Figure 1.1 shows the turbine components and fluid station represented in the model.

Several concepts and terms are provided as background. A steady-state energy balance on a control volume gives

$$\dot{m}(h_1 + \tfrac{1}{2}V_1^2) + \dot{Q} = \dot{m}(h_2 + \tfrac{1}{2}V_2^2) \tag{1}$$

where *1* is inlet and *2* is outlet.

The total specific enthalpy is defined as

$$h_t = h + \tfrac{1}{2}V^2 . \tag{2}$$

Hence, the change in total specific enthalpy between inlet and outlet is

$$H = h_2 + \tfrac{1}{2}V_2^2 - (h_1 + \tfrac{1}{2}V_1^2) . \tag{3}$$

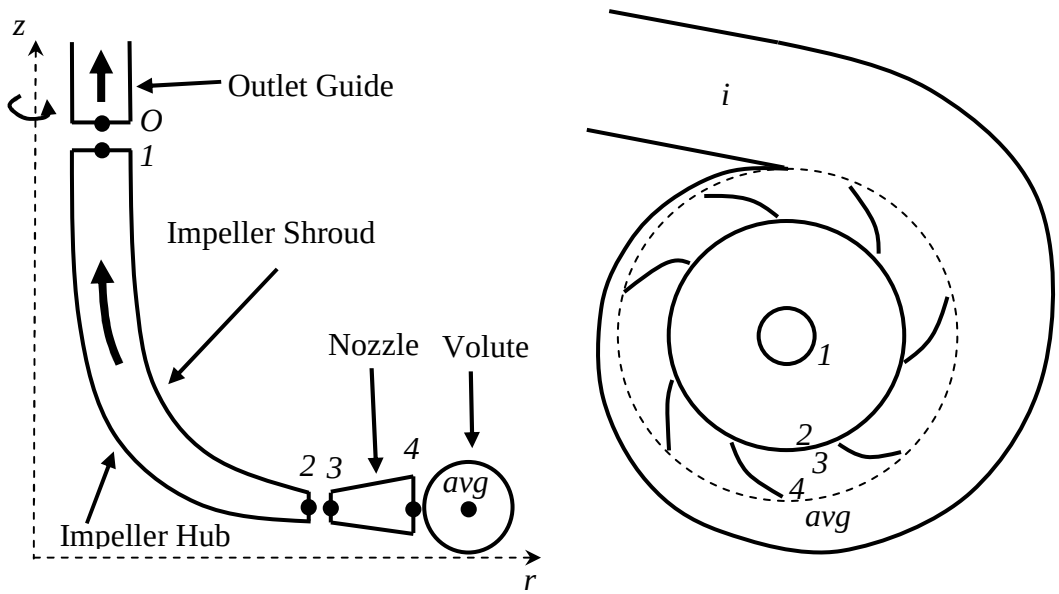

Figure 1.1 Radial Turbine Components and Stations. Left panel: cross-sectional view. Right panel: Overview from top.

The total specific enthalpy is from Eqs. (1) and (3) related to the mechanical work performed on the control volume and the mass flow rate through

$$H = \frac{\dot{Q}}{\dot{m}}. \tag{4}$$

The total pressure is defined as

$$P_t = P + \frac{1}{2}\rho V^2. \tag{5}$$

For no shaft work or gravitational work define the loss term h_{loss} through

$$\rho\, h_{loss} = P_{1t} - P_{2t}. \tag{6}$$

The nature of h_{loss} is seen by noting that

$$h_{loss} = \frac{P_1}{\rho} + \frac{1}{2}V_1^2 - \left(\frac{P_2}{\rho} + \frac{1}{2}V_2^2\right) = u_2 - u_1. \tag{7}$$

Thus h_{loss} represents the conversion of dynamic pressure between inlet and outlet into change in fluid internal energy (i.e. temperature) resulting from irreversibilities. In practice, the loss term is derived from experiments.

2.1 Volute

A one-dimensional model for the volute is derived for the representation shown in Figure 2.1. This figure assumes a cylindrical coordinate system centered on the impeller axis of rotation. The station *avg* is taken to represent the average conditions in the volute.

Assume the mass flow rate in the volute varies linearly with azimuthal angle starting at the inlet at station *i* and ending where the volute cross-sectional area goes to zero. The mass flow rate at station *avg* is then given by

$$\dot{m}_{avg} = 1/2\, \dot{m}_i \tag{8}$$

$$V_{avg} = \frac{\dot{m}_{avg}}{A_{X-Vol-avg}\ \rho_{avg}} \tag{9}$$

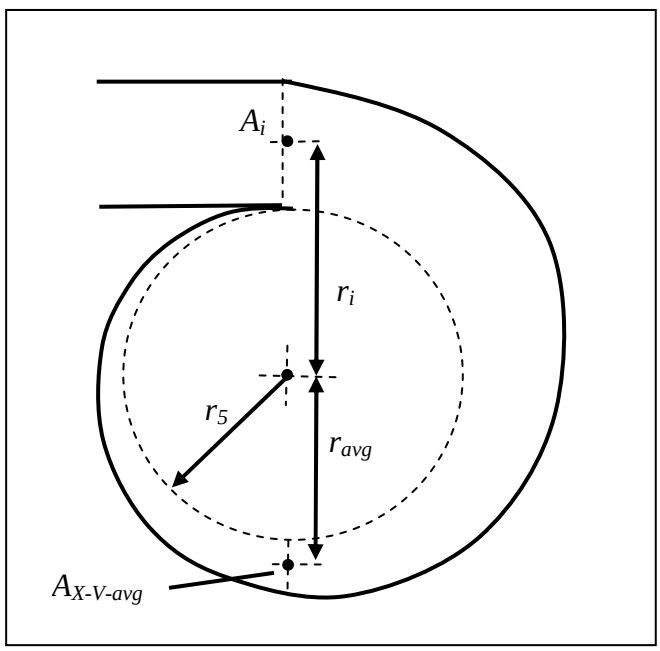

Figure 2.1 Dimension Variables for Volute

To estimate the azimuthal component of the velocity at station *5*, assume no losses in the volute so that angular momentum on a unit mass basis is conserved. Then this velocity is given by

$$V_{\theta-5} = \frac{V_{avg}\ r_{avg}}{r_5}. \tag{10}$$

A *circumferential distribution loss* is attributed to mixing in the volute resulting from non-uniform angular momentum at the volute exit and is given by [2]

$$P_{ti} - P_{t5} = \left(\frac{\frac{V_i\ r_i}{r_5} - V_{\theta-5}}{V_5} \right)^2 (P_{t-avg} - P_{avg}) \tag{11}$$

so that

$$h_{loss-V-cd} = \left(\frac{\frac{V_i\ r_i}{r_5} - V_{\theta-5}}{V_5} \right)^2 1/2 V_{avg}{}^2. \tag{12}$$

The friction loss in the volute is given by

$$P_{ti} - P_{t5} = f_{Vol} \frac{L_{Vol}}{D_{h-Vol}} (P_{t-avg} - P_{avg}) \tag{13}$$

where

$$D_{h-Vol} = (4A_{X-Vol-avg} / \pi)^{0.5} \tag{14}$$

so that

$$h_{loss-Vol-f} = \frac{C\ L_{Vol}}{2D_{h-Vol}{}^{1+n}} \left(\frac{\mu}{\rho} \right)^n V_{avg}{}^{2-n}. \tag{15}$$

Conservation of mass at the exit of the volute gives

$$V_{r-5} = \frac{\dot{m}_i}{A_{exit-Vol}\ \rho_{avg}} \tag{16}$$

where V_{r-5} is the radial component of the velocity at station *5*. The velocity at station *5* is then given by

$$V_5{}^2 = V_{r-5}{}^2 + V_{\theta-5}{}^2 \tag{17}$$

and the exit angle by

$$\alpha_5 = \sin^{-1}\left(\frac{V_{r-5}}{V_5}\right). \tag{18}$$

2.2 Nozzle

A schematic of the nozzle is shown in Figure 2.2. Geometric parameters that appear in the model are shown in the figure.

2.2.1 Exit Velocity Angle

The fluid upon passing the throat of the nozzle encounters an open area where the velocity is not well guided by the nozzle vanes. The angle at which the fluid exits the nozzle, i.e. the angle at which the fluid crosses the surface represented by radius r_3 , is estimated from the conservation of angular momentum. If losses are ignored, then the angular velocity of the fluid passing though the throat is related to that exit the nozzle by

$$v_{th-\theta}\, r_{th} = v_{3-\theta}\, r_3 . \tag{19}$$

The radial component of the velocity at the exit is given by

$$v_{3-r} = v_{3-\theta} \tan \alpha_3 \tag{20}$$

where α is the angle of the fluid velocity to the tangent.

From continuity of mass assuming density is constant

$$b_{th}\, w_{th}\, v_{th-\theta} \cos \beta_{th} = v_{3-r}\, b_3\, 2r_3 \sin\frac{\pi}{n} . \tag{21}$$

Combining the above three equations, the fluid exit angle is given by

$$\tan \alpha_3 = \frac{b_{th}\, w_{th} \cos \beta_{th}}{2\, b_3\, r_{th} \sin\frac{\pi}{n}} . \tag{22}$$

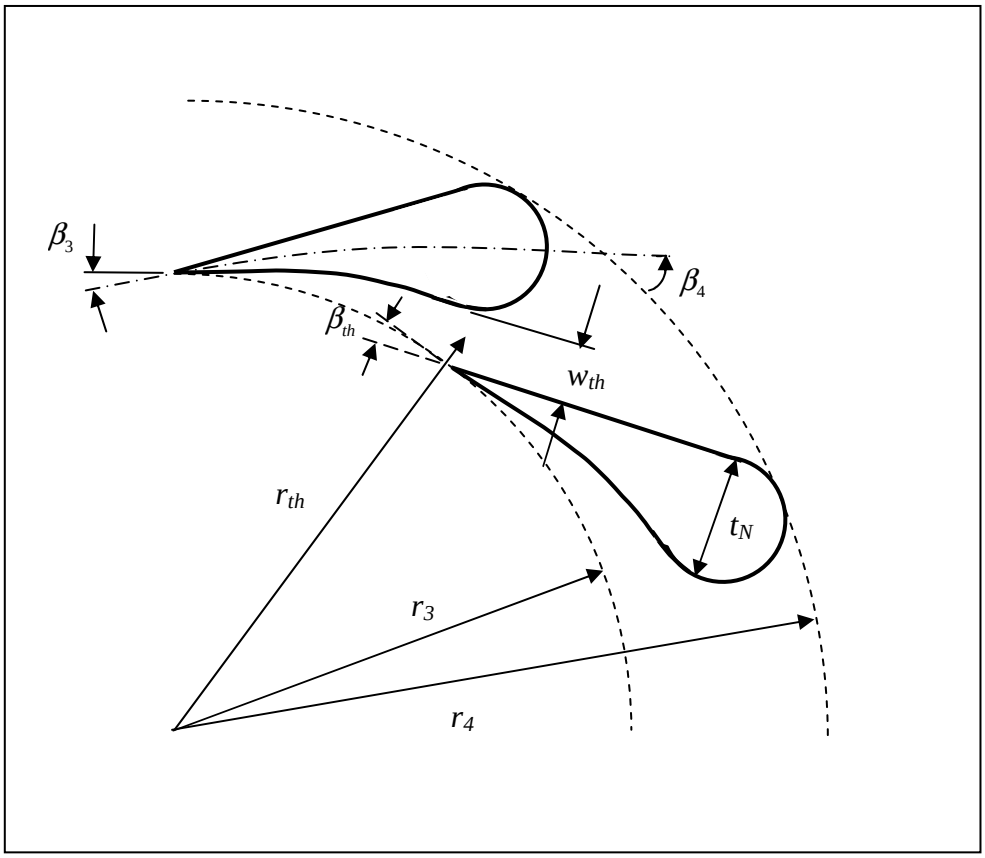

Figure 2.2 Schematic of Nozzle Geometric Parameters

2.2.2 Incident Loss

NASA Model - Fluid entering the nozzle undergoes an abrupt change in direction as it is channeled between the blades. In Figure 2.3 the absolute velocity changes from V_5 to V_4. A head loss occurs where it is assumed that the kinetic energy of the component of the velocity vector tangential to the nozzle of the fluid entering the nozzle is destroyed. [3] This velocity component appears as $V_{N||}$ in Figure 2.4. The total pressure loss is

$$\Delta P_{t-N-inc} = \frac{1}{2} f_{N-inc} \rho V_{N\|}^{2} \tag{23}$$

where $f_{N\text{-}inc}$ is 0.5 - 0.7. [4,5]

Application of the Law of the Sines to Figure 3 gives

$$\frac{\sin x}{V_{N\|}} = \frac{\sin \beta_4}{V_5}. \tag{24}$$

Then from Figure 2.4 and the equation

$$V_{N\|} = V_5 \frac{\sin(\pi - \alpha_5 - \beta_4)}{\sin \beta_4}. \tag{25}$$

$$V_4 = V_5 \frac{\sin \alpha_5}{\sin \beta_4}$$

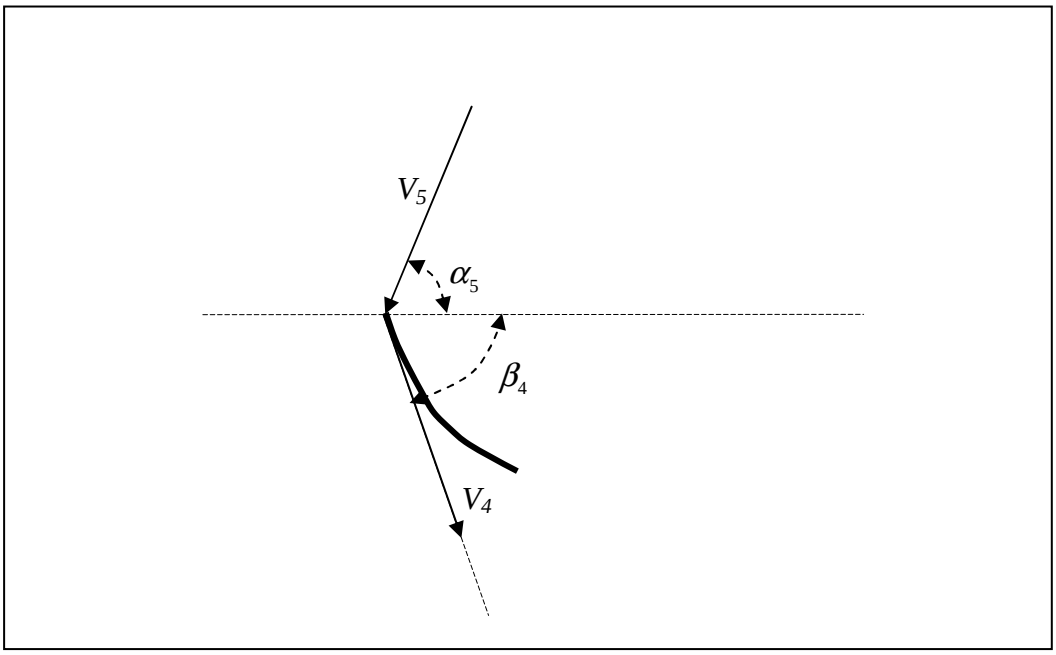

Figure 2.3 View of Blade at Nozzle Inlet

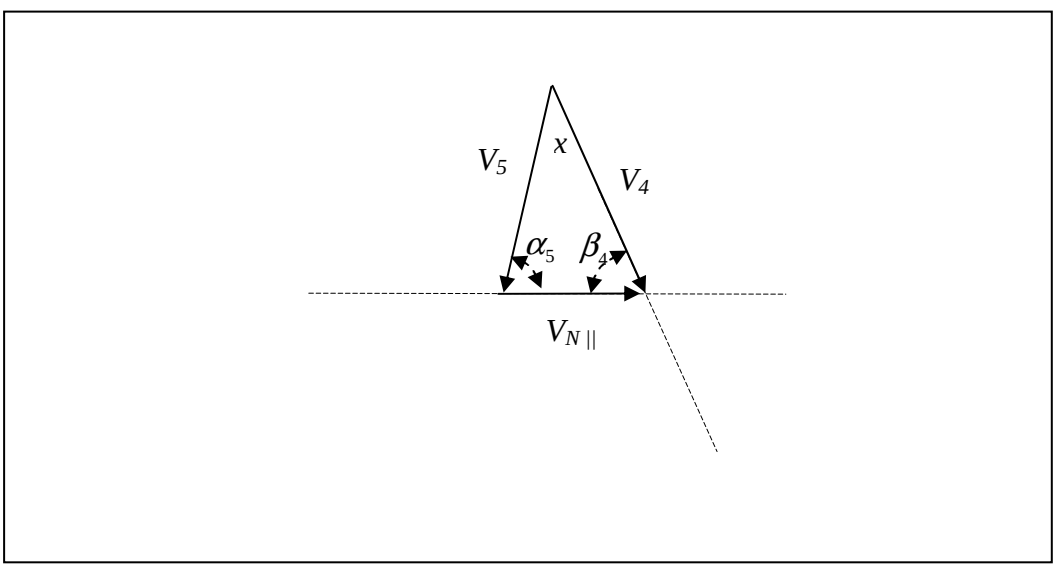

Figure 2.4 Nozzle Inlet Velocity Triangles

Aungier Model – An alternate model for the nozzle loss is given in [2]. The optimum incidence angle, i^*, and inlet flow angle, α^*, are given by

$$i^* = \left[3.6\sqrt{10\,t_N / L} + \frac{|\beta_3 - \beta_4|}{3.4}\right]\sqrt{L\frac{n}{2\pi r_3}} - \frac{|\beta_3 - \beta_4|}{2}$$

$$\alpha^* = \beta_4 - i^*\, sign(\beta_3 - \beta_4) \tag{26}$$

The total pressure loss is then

$$\Delta P_{t-N-inc} = (P_{t4} - P_4)\sin^2(\alpha_4 - \alpha^*) \tag{27}$$

2.2.3 Form Loss

The form loss is given by Rogers as reported in [6] and accounts for the geometry of the nozzle. The loss is given by

$$h_{loss-N-f} = \mathrm{Re}_N^{-1/5}\,\Psi_N\,\frac{1}{2}V_3^{\,2} \tag{28}$$

where

$$\Psi_N = \frac{1}{20}\left(\frac{3\sin\alpha_4}{s_3 / c} + \frac{w_{th}}{b_{th}}\right) \tag{29}$$

where s is the nozzle vane pitch at the trailing edge, c is the chord length of the nozzle vane, and

$$\mathrm{Re} = \frac{V_3\, b_3}{\mu_3 / \rho_3\,|_{first}}\,. \tag{30}$$

2.3 Impeller

2.3.1 Head

An expression for the change in fluid total specific enthalpy imparted to the impeller is given in the Appendix as

$$H_I = U_2 V_{2||} - U_1 V_{1||} \tag{31}$$

or

$$H_I / U_2^{\,2} = (U_2 V_{2||} - U_1 V_{1||}) / U_2^{\,2} \tag{32}$$

But also from the Appendix Eq. (A.9) (assuming the relative velocity of the fluid entering and exiting the impeller is parallel to the blade)

$$V_{1||} = U_1 + \frac{\dot{m}}{2\pi\, r_1\, b_1\, \rho_1} \cot \beta_1 \tag{33}$$

and

$$V_{2||} = U_2 + \frac{\dot{m}}{2\pi\, r_2\, b_2\, \rho_2} \cot \beta_2 \cdot \tag{34}$$

So Eq. (32) becomes

$$H_I = (1 + \frac{\dot{m}}{2\pi\, r_2\, b_2\, \rho_2 U_2} \cot \beta_2)\, U_2^{\,2} - (1 + \frac{\dot{m}}{2\pi\, r_1\, b_1\, \rho_1 U_1} \cot \beta_1) U_1^{\,2} \tag{35}$$

In the special case where the fluid exits the eye of the impeller parallel to the axis of rotation, then the fluid has no momentum in the plane of rotation. In this case Eq. (35) simplifies to

$$H_I = 1 + \frac{\dot{m}}{2\pi\, r_2\, b_2\, \rho_2 U_2} \cot \beta_2\, U_2^{\,2} . \tag{36}$$

2.3.2 Incidence Loss

The total pressure loss associated with fluid incident on the impeller blade is given as a function of the inlet velocity angle, α_2 , by [2]

$$\Delta P_{t-I-inc} = (P_{t2} - P_2) \sin^2(\alpha_2 - \alpha_2 *) \tag{37}$$

where

$$V_{\theta 2} * = \sigma \left(U_2 - \quad V_{m2} \cot \beta_2 \right)$$

$$\cot \alpha_2 * = \frac{V_{m2}}{V_{\theta 2} *} . \tag{38}$$

If the fluid enters with no axial velocity component (i.e. normal to the axis of rotation), then $V_{m2} = V_{r2}$.

A correlation for the slip factor σ appears in [2]

$$\sigma = 1 - \sqrt{\sin\beta_1}\,\sin\gamma_1 / n^{0.7}\,. \tag{39}$$

For the case of splitter blades

$$n = n_{fb} + n_{sb}\, L_{sb}/L_{fb} \tag{40}$$

where L is the meridional length of the blade and subscripts *fb* and *sb* represent full blade and short blade, respectively. The limiting radius must be checked for both long and short blades.

There is an upper limit for the value of the impeller mean-line radius ratio for which Eq. (39) is valid. Beyond that value a correction factor must be applied to the slip factor. The impeller mean-line radius ratio is given by

$$\varepsilon = \frac{r_{1-inner} + r_{1-outer}}{2r_2} \tag{41}$$

where subscript *inner* denotes the inner radius of the blade and the subscript *outer* denotes the outer radius of the blade, both at the impeller outlet. The upper limit is from [2]

$$\varepsilon_{\lim} = \frac{\sigma - \sigma^*}{1 - \sigma^*} \tag{42}$$

where

$$\sigma^* = \sin(19^\circ + 0.2\beta_1)\,. \tag{43}$$

If $\varepsilon > \varepsilon_{lim}$, then the slip factor is replaced by the corrected slip factor

$$\sigma_{corr} = \sigma\,(1 - \zeta) \tag{44}$$

where

$$\zeta = \left[\frac{\varepsilon - \varepsilon_{\lim}}{1 - \varepsilon_{\lim}}\right]^{\sqrt{\beta_1/10}}\,. \tag{45}$$

2.3.3 Channel-Flow Friction Loss

The losses in the impeller while multi-dimensional are assumed to behave as those in a one-dimensional channel where the shear stress is given by the friction factor adjusted according to the concept of the hydraulic diameter. The total pressure loss is

$$\Delta P_{t-I-f} = f \frac{L_I}{D_{h-I}} \rho \frac{W^2}{2} \tag{46}$$

where L is the channel length, D_h is the channel hydraulic diameter, and W is relative velocity. Assume $f = C\,Re^{-n}$ where Re is the Reynolds number and C and n are constants. Then Eq. (46) becomes

$$\Delta P_{t-I-f} = \frac{C\,L_I}{2D_{h-I}^{\;1+n}} \mu^n \rho^{1-n} W^{2-n} \tag{47}$$

or

$$h_{loss-I-f} = \frac{CL_I}{2D_{h-I}^{\;1+n}} \left(\frac{\mu}{\rho}\right)^n W^{2-n}. \tag{48}$$

The relative velocity is taken as the average of the relative velocities at the inlet and outlet

$$W = \frac{W_2 + W_1}{2} \tag{49}$$

where from Figure 2.5

$$W_{2-\theta} = V_2 \cos\alpha_2 - U_2$$
$$W_{2-r} = V_2 \sin\alpha_2$$
$$W_2 = \sqrt{W_{2-\theta}^{\;2} + W_{2-r}^{\;2}}$$

and

$$W_{1-\theta} = V_1 \cos\alpha_1 - U_1$$
$$W_{1-r} = V_1 \sin\alpha_1$$
$$W_1 = \sqrt{W_{1-\theta}^{\;2} + W_{1-r}^{\;2}}$$

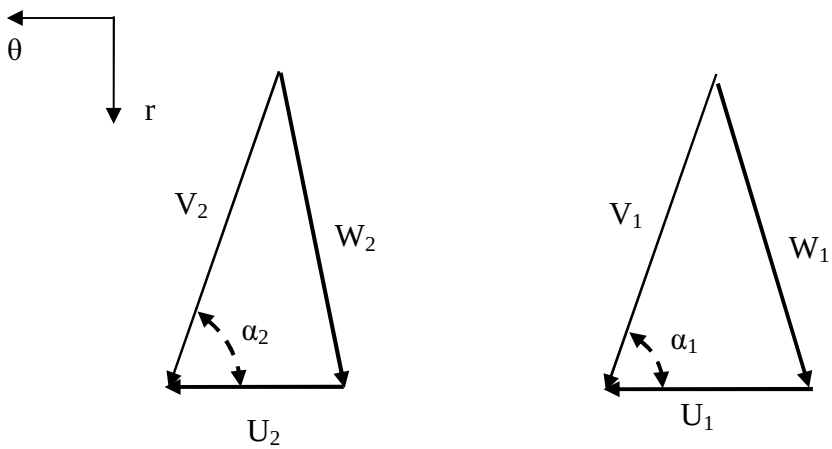

Figure 2.5 Impeller Velocity Triangles

2.3.4 Blade-Loading Loss

The model for total pressure loss due to wall shear stress given above is based on a one-dimensional idealization for fluid flow down the channel formed by adjacent blades. However, the pressure distribution normal to this direction is not uniform but exhibits higher pressure in back of a blade compared to in front of the blade. A "blade loading loss" in conjunction with the one-dimensional channel loss is needed to account for the observed head loss. [2,7]

From [3]

$$\Delta P_{t-I-bl} = (P_t - P)_2 (\Delta W / W_2)^2 / 24 \tag{50}$$

where ΔW is the relative velocity of the fluid at the pressure side of the blade minus that at the exhaust side and is given by the expression [7]

$$\Delta W = \frac{2\pi d_2 H_t}{n U_2 L} \tag{51}$$

and where H_t is the specific enthalpy change induced by the impeller and is given by Eq. (36). Then From Eq. (50)

$$h_{loss-bl} = \frac{1}{\rho} (P_t - P)_2 (\Delta W / W_2)^2 / 24 \tag{52}$$

2.3.5 Blade-Leakage Loss

The impeller blades mate up against the turbine housing with a small clearance to avoid intimate contact. In addition the fluid pushes on the leading surface of each blade essentially

creating a pressure difference between the leading and trailing blade leading surfaces i.e. across the blade. This difference in pressure gives rise to a flow through the blade-housing clearance gap. This flow results in pressure dissipation and a consequent loss.

An expression for the loss is derived. The fluid velocity through the clearance is linked to the pressure difference across the clearance through a expression given in [3,7]

$$\Delta P_{cl} = 1.5 \cdot \tfrac{1}{2} \rho U_{cl}{}^{2}, \text{ or } U_{cl} = 0.816 \cdot (2\Delta P_{cl} / \rho)^{1/2} \tag{53}$$

The loss coefficient in the above expression (i.e. K = 1.5) is based on an abrupt contraction in series with an abrupt expansion.

The pressure decrease across the blades causes a force on the blades so that mechanical work is done to the blades as they move. The mechanical power delivered by the fluid is

$$\omega T = \omega \cdot \bar{r} \cdot n \bar{b} \, L \, \Delta P_{cl} \tag{54}$$

where the third and last term on the right hand side is the total force exerted by the fluid normal to the blades. But the mechanical power of the blades appears as the specific enthalpy decrease through the turbine times the mass flow rate so that from the above expressions

$$\dot{m} H_I = \omega \cdot \bar{r} \cdot n \bar{b} \, L \, \Delta P_{cl} \tag{55}$$

Rearranging

$$\Delta P_{cl} = \frac{\dot{m} H_I}{\omega \cdot \bar{r} \cdot n \bar{b} \, L} \tag{56}$$

where ω is rad/s. Unproductive shaft mechanical power lost due to clearance leakage equals the pumping power through the clearance

$$\dot{m}_{cl} \, \Delta P_{cl} / \rho = \dot{m} \, h_{loss-I-cl} \tag{57}$$

or

$$h_{loss-I-cl} = \frac{\dot{m}_{cl} \, \Delta P_{cl}}{\rho \, \dot{m}} \tag{58}$$

In the above expression the mass flow rate through the clearance is given by the mass balance

$$\dot{m}_{cl} = n \, s \, L \, \rho U_{cl} \tag{59}$$

Thus, the specific enthalpy lost to flow through the clearance gap can be calculated from Eq. (58) by first calculating gas pressure loss from Eq. (56), gap fluid velocity from Eq. (53) and finally gap mass flow rate from Eq. (59).

2.3.6 Efficiency

The impeller efficiency is defined as the ratio of shaft work with losses to that without losses

$$\eta_I = \frac{h_{t2} - h_{t1}}{h_{t2} - h_{t1}'} \tag{60}$$

where the prime superscript denotes a terminal state arrived at reversibly. That is

$$s_{t1}' = s_{t2} \tag{61}$$

where it is assumed the terminal total pressure, P_{t1} , is the same whether the terminal state is arrived at irreversibly or reversibly. From properties

$$s_{t2} = f_{P,H\to S}(P_{t2}, h_{t2}) . \tag{62}$$

But

$$h_{t1}' = f_{P,S\to h}(P_{t1}, s_{t1}') \tag{63}$$

so that

$$h_{t1}' = f_{P,S\to h}(P_{t1}, s_{t2}) . \tag{64}$$

The losses equal the maximum work minus the actual work

$$h_{I-loss} = (h_{t2} - h_{t1}') - (h_{t2} - h_{t1}) . \tag{65}$$

Inserting this equation into the definition of efficiency above

$$\eta_I = \frac{h_{t2} - h_{t1}}{(h_{t2} - h_{t1}) + h_{I-loss}} \tag{66}$$

and rearranging the equation for the definition of efficiency

$$h_{t1} = h_{t2} - \eta_I (h_{t2} - h_{t1}') . \tag{67}$$

2.4 Outlet

The fluid exiting the impeller and entering the impeller eye undergoes a loss represented by

$$P_{t1} = P_{t0} + h_{loss-O-contr} \tag{68}$$

For the case where the loss is represented by an abrupt area decrease

$$h_{loss-O-contr} = \left(\frac{1}{C} - 1\right)^2 \frac{1}{2} \rho v_0^{\,2} \tag{69}$$

where v_0 is the average coolant velocity in the contracted channel and C is the *contraction coefficient* and is given by [8]

$$C = 0.63 + 0.37 \left(A_0 / A_1\right)^3 . \tag{70}$$

2.5 Parasitic Losses

2.5.1 Windage

The back face of the impeller hub is an annular disk that spins with the impeller. This disc may either mate with a fixed surface separated from it by a small clearance or it may spin freely far from other fixed surfaces. In either case the fluid contacting the disc exerts a shear on the disc with result that the fluid does unproductive work. This loss of power is referred to as windage loss. The following method for calculating it is given in [7].
The disk torque coefficient is defined by

$$C_M = \frac{2\tau}{\rho \omega^2 r^5} , \tag{71}$$

where τ is the torque.

A Reynolds number Re is defined

$$\mathrm{Re} = \frac{\rho \omega r^2}{\mu} \tag{72}$$

where r is the radius of the disk. If s is the clearance between the back of the impeller and the turbine body, then assuming a turbulent flow regime

$$C_M = \frac{0.102 (s / r)^{0.1}}{\mathrm{Re}^{0.2}} . \tag{73}$$

Then it follows that the specific head loss is

$$h_{loss-I-wd} = \frac{\omega\tau}{\dot{m}} = \frac{\rho C_M U_2{}^3 r^2}{2\dot{m}} . \tag{74}$$

2.6 Solution Algorithm

The integrated turbine behavior is obtained by collecting the governing equations and solving them such that each equation is simultaneously satisfied. The manner in which the equations are solved depends on the boundary conditions. If the boundary conditions are prescribed at the inlet to the turbine, then subsets of equations can be solved serially so that iteration on only two unknowns is needed. If, however, the model is to be incorporated in the GPASS code, then a more general set of boundary conditions must be accommodated. In this case an additional set of equations that interface the model to the rest of the plant system are solved simultaneously with the plant equations.

The development below assumes the first case above where the boundary conditions are represented by

$\dot{m}_i$	=	inlet mass flow rate,
P_i	=	inlet pressure,
h_i	=	inlet enthalpy, and
ω	=	shaft speed.

2.6.1 Volute

Calculate geometry dependencies:

$$r_5 = D_4 / 2$$

$$r_{avg} = \frac{r_i + r_5}{2}$$

$$A_{X-V-avg} = A_i / 2$$

$$D_{h-V} = (4A_{X-V-avg} / \pi)^{0.5}$$

Calculate:

$$\rho_i = f_{es}(h_i, P_i)$$

$$V_i = \frac{\dot{m}_i}{A_i \ \rho_i}$$

$$P_{ti} = P_i + 1/2 \ \rho_i V_i^2$$

$$h_{ti} = h_i + 1/2 \ V_i^2$$

$$\dot{m}_{avg} = 1/2 \ \dot{m}_i$$

Assume for transition from inlet to volute:

$$h_{t-avg} = h_{ti}$$

Iterate on V_{avg} :

$$\rho_{avg} \mid_{first} = \frac{\dot{m}_{avg}}{A_{X-Vol-avg} \ V_{avg}}$$

$$V_{\theta-5} = \frac{V_{avg} \ r_{avg}}{r_5}$$

$$V_{r-5} = \frac{\dot{m}_i}{A_{exit-Vol} \ \ \rho_{avg} \mid_{first}}$$

$$V_5^{\ 2} = V_{r-5}^{\ \ 2} + V_{\theta-5}^{\ \ 2}$$

$$h_{loss-V-cd} = \left(\frac{\frac{V_i \ r_i}{r_5} - V_{\theta-5}}{V_5} \right)^2 1/2 V_{avg}^{\ \ 2}$$

$$h_{loss-Vol-f} = \frac{C \ L_{Vol}}{2 D_{h-Vol}^{\ \ 1+n}} \left(\frac{\mu}{\rho} \right)^n V_{avg}^{\ \ 2-n}$$

$$P_{t-avg} = P_{ti} - \rho_{avg} \mid_{first} (h_{loss-V-f} + h_{loss-V-cd})$$

$$P_{avg} = P_{t-avg} - 1/2 \ \rho_{avg} \mid_{first} V_{avg}^{\ \ 2}$$

$$h_{avg} = h_{t-avg} - 1/2\, V_{avg}{}^2$$

$$\rho_{avg}\,|_{second} = f_{es}(h_{avg}, P_{avg})$$

Stop iterating if:

$$\rho_{avg}\,|_{second} - \rho_{avg}\,|_{first} < \varepsilon$$

Calculate:

$$\alpha_5 = \sin^{-1}\left(\frac{V_{r-5}}{V_5}\right)$$

2.6.2 Nozzle

Assume for transition from volute to nozzle:

$$\alpha_4 = \alpha_5$$

$$P_{t-4} = P_{t-avg}$$

$$\rho_4 = \rho_{avg}\,|_{first}$$

$h_{t3} = h_{t-avg}$ (adiabatic and no work done so total enthalpy is conserved)

Calculate geometry dependencies:

$$A_3 = \lambda_3 \pi D_3 b_3 \sin\beta_3$$

$$A_4 = \lambda_4 \pi D_4 b_4 \sin\beta_4$$

$$D_{h-Nf} = \frac{1}{2}\left[\frac{4A_3}{\lambda_3 2\pi D_3 + 2b_3 n_N} + \frac{4A_4}{\lambda_4 2\pi D_4 + 2b_4 n_N}\right]$$

Calculate:

$$V_4 = V_5\,\frac{\sin\alpha_5}{\sin\beta_4}$$

$$P_4 = P_{t-4} - 1/2\,\rho_4 V_4{}^2$$

$$i^* = \left[3.6\sqrt{10\, t_N / L} + \frac{|\beta_3 - \beta_4|}{3.4} \right] \sqrt{L \frac{n}{2\pi r_3}} - \frac{|\beta_3 - \beta_4|}{2}$$

$$\alpha^* = \beta_4 - i^* \, sign(\beta_3 - \beta_4)$$

$$h_{loss-N-inc} = \frac{1}{\rho_4} (P_{t4} - P_4) \sin^2(\alpha_4 - \alpha^*)$$

$$\Psi_N = \frac{1}{20} \left(\frac{3 \sin \alpha_4}{s_3 / c} + \frac{w_{th}}{b_{th}} \right)$$

$$\alpha_3 = \tan^{-1} \left(\frac{b_{th}\, w_{th} \cos \beta_{th}}{2\, b_3\, r_{th} \sin \frac{\pi}{n}} \right)$$

Iterate on V_3:

$$\rho_3 |_{first} = \frac{\dot{m}_i}{V_3 A_3}$$

$$\mathrm{Re}_N = \frac{V_3\, b_3}{\mu_3 / \rho_3 |_{first}}$$

$$h_{loss-N-f} = \mathrm{Re}_N^{-1/5}\, \Psi_N \frac{1}{2} V_3^2$$

$$h_3 = h_{t3} - \frac{1}{2} V_3^2$$

$$P_{t3} = P_{t4} - \rho_3 |_{first} \, (h_{loss-N-inc} + h_{loss-N-f})$$

$$P_3 = P_{t3} - 1/2\, \rho_3 |_{first}\, V_3^2$$

$$\rho_3 |_{second} = f_{es}(h_3, P_3)$$

Stop iterating if:

$$\rho_3 |_{second} - \rho_3 |_{first} < \varepsilon$$

2.6.3 Impeller

Calculate geometry dependencies:

$$A_1 = \lambda_1 \frac{\pi}{4}(D_{1o}{}^2 - D_{1i}{}^2)\sin\beta_1 \quad \text{, where } \lambda_1 = \frac{1}{v_1}$$

$$A_{1-disc} = A_1 / \sin\beta_1$$

$$A_2 = \lambda_2 \pi D_2 b_2 \sin\beta_2 \text{, where } \lambda_2 = \frac{1}{v_2}$$

$$D_{h-I-f} = \frac{1}{2}\left(\frac{4A_1}{\lambda_1\pi(D_{1i}+D_{1o})+2b_1n_1} + \frac{4A_2}{\lambda_2 2\pi D_2 + 2b_2n_2}\right)$$

$$n = n_{fb} + n_{sb}L_{sb} / L_{fb}$$

$$\sigma = 1 - \sqrt{\sin\beta_1}\sin\gamma_1 / n^{0.7}$$

$$\sigma^* = \sin(19^\circ + 0.2\beta_1)$$

$$\varepsilon_{\lim} = \frac{\sigma - \sigma^*}{1 - \sigma^*}$$

$$\varepsilon = \frac{r_{1-inner} + r_{1-outer}}{2r_2}$$

$$\zeta = \left[\frac{\varepsilon - \varepsilon_{\lim}}{1 - \varepsilon_{\lim}}\right]^{\sqrt{\beta_1/10}}$$

$$\sigma_{corr} = \sigma\,(1 - \zeta)$$

$$\text{if } \varepsilon > \varepsilon_{lim}\text{, then } \sigma = \sigma_{corr}$$

Assume for transition from nozzle to impeller:

$$V_2 = V_3$$

$$P_{t2} = P_{t3}$$

$$\alpha_2 = \alpha_3$$
$$\rho_2 = \rho_3$$

$$h_{t2} = h_{t3}$$

Calculate:

$$V_{r2} = V_2 \sin\alpha_2$$

$$V_{m2} = V_{r2}$$

$$V_{\theta 2}* = \sigma\left(U_2 - \quad V_{m2}\cot\beta_2\right)$$

$$\cot\alpha_2* = \frac{V_{m2}}{V_{\theta 2}*}$$

$$W_{2-\theta} = V_2\cos\alpha_2 - U_2$$
$$W_{2-r} = V_2\sin\alpha_2$$
$$W_2 = \sqrt{W_{2-\theta}{}^2 + W_{2-r}{}^2}$$

$$P_2 = P_{t2} - \frac{1}{2}\rho_2 V_2{}^2$$

$$h_{loss-I-inc} = \frac{1}{\rho_2}(P_{t2} - P_2)\sin^2(\alpha_2 - \alpha_2*)$$

$$s_{t2} = f_{P,H\to S}(P_{t2}, h_{t2})$$

Iterate on $\rho_1|_{first}$ and V_1 :

$$H_I = (1 + \frac{\dot{m}}{2\pi r_2 b_2 \rho_2 U_2}\cot\beta_2)U_2{}^2 - (1 + \frac{\dot{m}}{2\pi r_1 b_1 \rho_1 U_1}\cot\beta_1)U_1{}^2$$

$$\Delta W_I = \frac{2\pi d_2 H_I}{nU_2 L}$$
$$V_{1r} = \frac{\dot{m}}{\rho_1|_{first} A_{1-disc}}$$

$$\alpha_1 = \sin^{-1}\left(\frac{V_{1r}}{V_1}\right)$$

$$W_{1-\theta} = V_1 \cos\alpha_1 - U_1$$
$$W_{1-r} = V_1 \sin\alpha_1$$
$$W_1 = \sqrt{W_{1-\theta}{}^2 + W_{1-r}{}^2}$$

$$\overline{W}_I = \frac{W_2 + W_1}{2}$$

$$\overline{\rho} = \left(\rho_2 + \rho_1|_{first}\right)/2$$

$$h_{loss-I-bl} = \frac{1}{\overline{\rho}}\left(P_{t2} - P_2\right)(\Delta W_I / \overline{W}_I)^2 / 24$$

$$h_{loss-I-f} = \frac{CL_I}{2D_{h-I}{}^{1+n}}\left(\frac{\mu}{\overline{\rho}}\right)^n \overline{W}_I{}^{2-n}$$

$$h_{t1}|_{first} = h_{t2} - H_t$$

$$h_1 = h_{t1}|_{first} - \frac{1}{2}V_1^2$$

$$P_1 = f_{h,\rho\to P}\left(h_1, \rho_1|_{first}\right)$$

$$P_{t1} = P_1 + \frac{1}{2}\rho_1|_{first} V_1^2$$

$$\rho_1|_{second} = \frac{\dot{m}}{W_1 A_1}$$

$$\Delta P_{cl} = \frac{\dot{m} H_I}{\omega \cdot \overline{r} \cdot n\overline{b} L}$$

$$U_{cl} = 0.816 \cdot (2\Delta P_{cl} / \overline{\rho})^{1/2}$$

$$\dot{m}_{cl} = n s L \overline{\rho} U_{cl}$$

$$h_{loss-I-cl} = \frac{\dot{m}_{cl}\,\Delta P_{cl}}{\bar{\rho}\,\dot{m}}$$

$$h_{I-loss} = h_{loss-I-inc} + h_{loss-I-f} + h_{loss-I-bl} + h_{loss-I-cl}$$

$$\eta_I = \frac{h_{t2} - h_{t1}|_{first}}{(h_{t2} - h_{t1}|_{first}) + h_{I-loss}}$$

$$h_{t1}' = f_{P,S\to h}(P_{t1}, s_{t2})$$

$$h_{t1}|_{\text{second}} = h_{t2} - \eta_I (h_{t2} - h_{t1}')$$

Stop iterating if:

$$h_{t1}|_{first} - h_{t1}|_{second} = 0$$

$$\rho_1|_{first} - \rho_1|_{second} = 0$$

3 Validation

The turbine model is validated by comparing model predictions with experiment data. The data are from a test performed at Barber-Nichols for a loop configuration referred to as the Simple Split-Flow Recuperated Brayton Cycle. A schematic of this loop is shown in Figure 3.1. In the test the heater power and shaft speed were increased in a step-like fashion with each step held long enough that the loop reached steady state. The specific data analyzed are from the turbine designated T2 mounted on the main compressor shaft designated TAC-A. See Table 3.1 for the designation of all turbomachines and their respective shafts. The test was performed on December 1, 2010 and was labeled as Test 101201-1041.

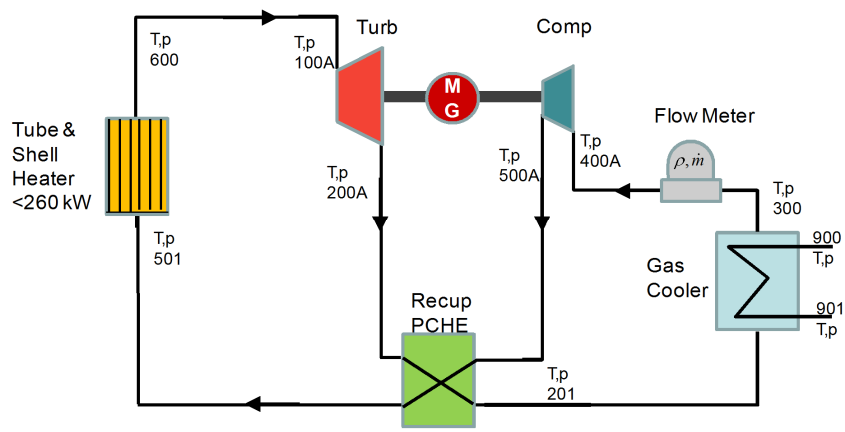

Figure 3.1 Simple Split-Flow Recuperated Brayton Cycle Layout of Test 101201-1041 (Courtesy of SNL)

Table 3.1 Turbine-Alternator-Compressor (TAC) Shafts and Associated Turbomachine Identities

TAC Shaft	Turbine	Compressor
TAC-A	T-2	C-1 (main compressor)
TAC-B	T-3	C-2 (recompressor)

The geometric data for the turbine are given in Tables 3.2 through 3.4. These data were taken from engineering drawings of the turbine.

Table 3.2 Volute Geometry Parameters for Turbine T-2 for Main Compressor

r_i	Radial distance from shaft center line to middle of volute inlet	not applicable
A_i	Cross sectional flow area at volute inlet	not applicable

Table 3.3 Nozzle Geometry Parameters for Turbine T-2 for Main Compressor

β_4	Angle between vane and wheel tangent at nozzle inlet, degrees	39
β_{th}	Angle of nozzle throat to tangent passing through the nozzle, degrees	17
β_3	Angle between vane and tangent at nozzle outlet, deg	13
N_N	Number of vanes in nozzle	10
D_4	Diameter at inlet to nozzle, m	$((1.66^2+0.388^2)^{0.5}+0.1725)$ *2*2.54e-2=0.0954
D_{th}	Diameter at nozzle throat, m	0.0732
D_3	Diameter at outlet of nozzle, m	1.374*2*2.54e-2=0.0698
b_4	Height of vane at nozzle inlet, m	0.15*2.54e-02=0.0038
b_{th}	Height of vane at throat, m	0.0038
b_3	Height of vane at nozzle outlet, m	0.0038
L_N	Length of flow channel from nozzle inlet to outlet	0.02
c	Cord length of vane, m	0.0303
t_N	Thickness of vane, m	0.009
w_{th}	Width of nozzle throat, m	0.0033
λ_4	Void fraction at nozzle inlet (as fraction of circumference)	1.0
λ_3	Void fraction at nozzle outlet (as fraction of circumference)	1.0

Table 3.4 Impeller Geometry Parameters for Turbine T-2 for Main Compressor

β_2	Angle between blade and wheel tangent at impeller inlet, degrees	90
β_1	Angle between blade and wheel tangent at impeller outlet, degrees	150
Φ_{inc}	Angle at outlet between streamline and plane normal to axis of rotation, degrees	NA
n_2	Number of blades at impeller inlet	11
n_1	Number of blades at impeller outlet	11
$D_{I\text{-}2}$	Diameter of impeller at inlet, m	0.0676
$D_{I\text{-}1i}$	Impeller outlet inner diameter, m	0.2515*2*2.54e-02=0.0128
$D_{I\text{-}1o}$	Impeller outlet outer diameter, m	0.628*2*2.54e-02=0.0319
b_2	Height of blade at impeller inlet, m	0.1715*2.54e-02=0.0044
b_1	Length of blade edge at impeller outlet, m	(0.628-0.2515)*2.54e-02=0.0096
L_I	Length of flow channel from impeller inlet to outlet, m	$\left(\left[(0.0676-(0.0128+0.0319)/2)/2\right]^2+0.02^2\right)^{1/2} = 0.03$
λ_2	Void fraction at impeller inlet given blade solidity (projected onto plane with normal parallel to direction of flow)	$1-\frac{7.1*10^{-4}*11}{\pi 0.0676}=0.96$
λ_1	Void fraction at impeller outlet given blade solidity (projected onto plane with normal parallel to direction of flow)	$1-\frac{7.1*10^{-4}}{\pi(0.0128+0.0319)/2/11*\sin\Phi_{inc}} = 0.78$
s	Gap between impeller blade and hub, m	0.005*0.0254=0.13e-03
γ_1	Angle between streamline and axis of rotation, degrees	60

3.1 Instrumentation

Boundary conditions for driving the turbine model were taken from sensors RPM1, FLOW, T100A, and P100A which measure turbine shaft speed, mass flow rate, inlet temperature (total) and inlet pressure (total), respectively.[9] The temperature and pressure sensors are located in the pipe schedule 1.5 in. line connected to the turbine inlet. The pressure head in this line at 25 kRPM is, based on the mass flow rate, 20kPa or about one-hundredth of the turbine pressure drop.

Measured quantities for comparison with turbine model outputs are available in the pipe schedule 1.5 in. line connected to the turbine outlet. Resistance temperature detector (RTD) T200A and pressure transducer P200A are located in this line and measure total temperature and pressure.

Instruments T100A and T200A are RTDs and are accurate to ± 0.2 ^{o}C while instruments P100A and P200A are accurate to ± 0.02 MPa.[10] Instrument FLOW is a Coriolis flow meter with a mass flow rate accuracy of better than ± 0.5 %.[10]

3.2 Sensitivity and Uncertainty Analysis

The accuracy of the turbine model is assessed by comparison with experiment data. The data itself is subject to uncertainty and so the affect of this on the comparison was first quantified. The model accuracy is evaluated with respect to two quantities, the specific enthalpy change across the turbine, Δh, and pressure change, ΔP. Table 3.5 shows how an error in either of the two boundary conditions, inlet temperature or pressure, perturb these quantities. For enthalpy change, there is both the predicted model value and the value calculated from measured temperature and pressure. The table gives sensitivity coefficients for a one percent perturbation in normalized turbine inlet temperature and inlet pressure.

Given the uncertainties specified in Section 3.1for the instrumentation, the data in Table 3.5 indicate that the resulting uncertainty in the model-based and measurement-based validation quantities is less than 0.2 percent. Note that validation of the turbine model is not subject to the large uncertainties in validation quantities which differs from the compressor model.[1] The sensitivity of S-CO_2 properties to temperature and pressure at turbine operating conditions are not nearly as large compared to near the critical point where the compressor operates.

Table 3.5 Sensitivity of Turbine Validation Quantities to Measurement Error

		Measurement Error	
Validation Quantities		$\frac{\delta P_{ti}}{\Delta P\|_0} = 1\% \Rightarrow$ $\delta P_{ti} = -0.678*10^{-2}$ MPa	$\frac{\delta T_{ti}}{\Delta T\|_0} = 1\% \Rightarrow$ $\delta T_{ti} = -10.2*10^{-2}$ ^{0}C
Model Based	$\frac{\delta \Delta P}{\Delta P\|_0}$	< 0.1%	< 0.01%
	$\frac{\delta \Delta h}{\Delta h\|_0}$	< 0.01%	< 0.01%
Measurement Based	$\frac{\delta \Delta h}{\Delta h\|_0}$	-0.1%	1.1%

* From experiment @25 kRPM: $\Delta P|_0$ = -0.678 MPa $\Delta T|_0$ = -10.2 ^{0}C $\Delta h|_0$ = -8.6 kJ/kg

3.3 Volute Heat Loss

The thermocouple for measuring turbine inlet temperature is located in the inlet pipe upstream of the turbine. It is believed that the actual temperature of the fluid entering the turbine nozzle is less than the value measured by the thermocouple as a result of heat losses through the walls of the volute. The volute wall is in close proximity to the armature casing which is cooled by water circulating through internal coolant channels. A heat conduction path thus exists between the volute and the cooled casing. As a consequence the coolant passing through the volute is cooled and enters the nozzle of the turbine at a lower temperature than is indicated by sensor T100A which is located upstream in the pipe that connects to the volute. A model is developed for predicting the temperature exiting the volute given the temperature entering the volute.

The flow rate of the heat conducted or "leaking" from the coolant to the volute wall is given by

$$Q_{leak} = h_{film-vol}\ A_{wall-vol}\ (T_{CO2-vol} - T_{wall-vol}) \tag{75}$$

where

$h_{film\text{-}vol}$	=	film heat transfer coefficient,
$A_{wall\text{-}vol}$	=	area of volute wall participating in heat leakage,
$T_{CO2\text{-}vol}$	=	mixed mean temperature of coolant in volute assuming perfect mixing, and
$T_{wall\text{-}vol}$	=	temperature of volute wall.

and

$$h_{film-vol} = \frac{k_{CO2}}{D_{h-vol}}\, 0.023\, \mathrm{Re}^{0.8}\ \mathrm{Pr}^{0.3} \tag{76}$$

where

k_{CO2}	=	thermal conductivity of carbon dioxide,
D_h	=	hydraulic diameter of inlet volute,
Re	=	Reynolds number, and
Pr	=	Prandtl number.

The temperature drop through the volute is then given the energy balance

$$Q_{leak} = \dot{m}\,(h_{CO2-in}(T_{ti}\,, P_{ti}) - h_{CO2-vol}) \tag{77}$$

where $\dot{m}$ is the carbon dioxide coolant mass flow rate and T_{ti} and P_{ti} are the carbon dioxide temperature and pressure entering the volute, respectively, and correspond to sensors T100A and P100A, respectively. The coolant inlet enthalpy and volute coolant mixed mean enthalpy are given by, respectively,

$$h_{CO2-in} = f_{T,P\to h}(T_{ti}, P_{ti}) \qquad \text{and} \tag{78}$$

$$h_{CO2-vol} = f_{T,P\to h}(T_{CO2-vol}, P_{ti}) .$$

The temperature drop between the wall of the volute and the water-cooled metal is given by

$$Q_{leak} = A_{X\,sect-path} \frac{k_{steel-path}}{l_{length-path}} (T_{wall-vol} - T_{H2O}) \tag{79}$$

where

$A_{Xsect\text{-}path}$	=	area of the cross-section normal to the direction of heat flow and through which the heat flows,
$k_{steel\text{-}path}$	=	conductivity of steel,
$l_{length\text{-}path}$	=	length of conduction path, and
T_{H2O}	=	temperature of the water.

This set of equations is solved for the CO_2 temperature at the exit of the volute, $T_{CO2\text{-}vol}$,

$$\begin{bmatrix} \dot{m}\ C_{p-CO2} & 0 & 1 \\ 0 & A_{X\,sect-path}\dfrac{k_{steel-path}}{l_{length-path}} & -1 \\ h_{film-vol}\ A_{wall-vol} & -h_{film-vol}\ A_{wall-vol} & -1 \end{bmatrix} \begin{bmatrix} T_{CO2-vol} \\ T_{wall-vol} \\ Q_{leak} \end{bmatrix} = \begin{bmatrix} \dot{m}\ C_{p-CO2}\ T_{ti} \\ A_{X\,sect-path}\dfrac{k_{steel-path}}{l_{length-path}} T_{H2O} \\ 0 \end{bmatrix}$$

given the temperature of the CO_2 entering the volute, T_{ti} , and the water temperature, T_{H2O} , both of which are measured.

An estimate for the heat loss at the volute is made using the data below. The geometric data are taken from engineering drawings of the TAC-A. Since the model is one-dimensional while the volute and conduction paths are more complex in shape, the data below should be considered approximate.

Table 3.6 Parameter Values for Volute Heat Loss Model at 25 kRPM

T_{ti} = 148.1 C
P_{ti} = 8.284 MPa
T_{H2O} = 15.0 C
C_{p-CO2} = 1192 J/kg-C @148 C, 8.29 MPa
$\dot{m}$ = 0.9734 kg/s

$A_{X\,sect-path}$ = π 0.06 *0.03 = 0.006 m^2 (inlet volute torus projected onto 2-D ring)

$k_{steel-path}$ = 17 W/m-C (stainless steel)

$l_{length-path}$ = 0.025 m

$A_{wall-vol}$ = π 0.06 *0.03 = 0.006 m^2 (2-D ring)

$A_{X\,sect-vol}$ = π/4 * 0.03^2 = 7*10^{-5} m^2 (inlet volute torus cross section)

D_{h-vol} = 0.03 m (diameter of inlet volute torus cross section)

μ_{CO2} = 2.76*10^{-5} Pa-s

k_{CO2} = 57 W/m-C

$\mathrm{Re} = \dot{m}_{CO2} D_{h-vol} / (\mu_{CO2}\ A_{X\,sect-vol})$ = 2.146*0.03/(2.76*10^{-5}*7*10^{-5}) = 33*10^6

$\mathrm{Pr} = C_{p-CO2}\mu_{CO2} / k_{CO2}$ = 5*10^{-4}

These data yield a volute heat loss of Q_{leak} = 2.14 kW and an inlet temperature change of δT_{ti} = -1.85 ^{0}C at the conditions in Table 3.6.

3.4 Comparison of Model with Data

The initial results comparing the model of Section 2 against data for test101201-1041 are shown in Table 3.7. These results do not include the heat loss from the volute model of Section 3.3. One sees from Table 3.7 that with respect to the validation metrics, the turbine model differs significantly from the measured data. The model error is shown in bold.

Table 3.7 Comparison of Turbine Model with Experiment Data

			Experiment 101201-1041 Cycle Points		
Measured Inlet Boundary Conditions	ω / RPM1 (kRPM)		25.00 (3397 s)	35.069 (4500 s)	39.14 (6100)
	$\dot{m}$ / FLOW (kg/s)		0.9734	1.631	1.630
	T_{ti} / T100A (C)		148.1	147.6	203.6
	P_{ti} / P100A (MPa)		8.284	9.125	9.365
Outlet Conditions	T_{t1} / T200A (C)	Experiment	137.9	130.1	182.1
		Model	137.1	124.7	178.7
	P_{t1} / P200A (MPa)	Experiment	7.606	7.584	7.584
		Model	7.260	6.909	6.989
Validation Metrics	$\boldsymbol{\Delta P}$ = P_{t1} - P_{ti} (MPa)	Experiment	-0.6780	-1.541	-1.781
		Model	-1.024	-2.216	-2.376
		Model Error	-0.346 (**51%**)	-0.675 (**44%**)	-0.595 (**33%**)
	$\boldsymbol{\Delta h}$ from T_{ti}, P_{ti}, T_{t1}, and P_{t1} (kJ/kg)	Experiment	-8.600	-12.91	-17.98
		Model	-7.678	-15.45	-19.41
		Model Error	0.922 (**-11%**)	-2.54 (**20%**)	-1.43 (**8.0%**)

The role of heat loss at the inlet of the turbine downstream of the inlet temperature sensor and its effect on this result was investigated. If there is significant heat loss, then the experiment-

derived value for Δh will not be indicative of the actual turbine specific enthalpy change. The measured value for inlet temperature, T_{ti}, was decreased by the predicted temperature drop due to volute heat loss calculated using the model of Section 3.3. The corrected measured inlet temperature is shown in Table 3.8.

The corrected measured inlet temperature from Table 3.8 was used as the new inlet temperature for the turbine model and the data in Table 3.7 were recomputed. In addition the Euler head was multiplied by the factor, f_{head} , whose value was set to 0.85. The results are shown in Table 3.9. The calculated enthalpy change is in good agreement with the experiment, however, the present model over predicts the pressure change.

Table 3.8 Corrected Inlet Temperature and Enthalpy Measurements after Modeling Heat Loss through Volute Wall

	Model Boundary Conditions (Measured)			Modeled Heat Loss and Temperature Drop			Corrected Measurements	
ω (kRPM)	P_{ti} (MPa)	T_{ti} (C)	$\dot{m}$ (kg/s)	Q_{leak} (kW)	C_{p-CO2} (J/kg-C)	$\delta T_{ti} = Q_{leak} / (\dot{m}\ C_{p-CO2})$	$T_{ti}\|_{corr}$ (C)	$\Delta h\|_{corr}$ (kJ/kg)
25K	8.284	148.1	0.9734	2.14	1192	-1.85	146.3	-6.449
35K	9.125	147.6	1.631	2.15	1224	-1.10	146.5	-11.56
39K	9.365	203.6	1.630	3.05	1162	-1.57	202.0	-16.12

Table 3.9 Turbine Model with Corrected Experiment Inlet Temperature and 0.85 Multiplicative Head Factor

			Experiment 101201-1041 Cycle Points		
Measured Inlet Boundary Conditions	ω / RPM1 (kRPM)		25.00 (3397 s)	35.069 (4500 s)	39.14 (6100)
	$\dot{m}$ / FLOW (kg/s)		0.9734	1.631	1.630
	$T_{ti}\|_{corr}$ / T100 (C) (corrected)		146.3	146.5	202.0
	P_{ti} / P100 (MPa)		8.284	9.125	9.365
Outlet Conditions	T_{t1} / T200 (C)	Experiment	137.9	130.1	182.1
		Model	136.9	127.2	181.0
	P_{t1} / P200 (MPa)	Experiment	7.606	7.584	7.584
		Model	7.411	7.237	7.343
Validation Metrics	$\boldsymbol{\Delta P}$ = P_{t1} - P_{ti} (MPa)	Experiment	-0.6780	-1.541	-1.781
		Model	-0.8730	-1.888	-2.022
		Model Error	-0.195 (**29%**)	-0.347 (**23%**)	-0.241 (**14%**)
	$\boldsymbol{\Delta h\|_{corr}}$ from $T_{ti}\|_{corr}$, P_{ti}, T_{t1}, and P_{t1} (kJ/kg)	Experiment	-6.449	-11.56	-16.12
		Model	-6.528	-13.07	-16.39
		Model Error	-0.079 (**1%**)	-1.510 (**13%**)	-0.270 (**2%**)

To bring the pressure change into better agreement the pressure loss in the model was multiplied by the factor, f_{head} , whose value was set to 0.5. The result is shown in Table 3.10. The agreement on outlet pressure has improved.

Table 3.10 Turbine Model with Corrected Experiment Inlet Temperature, 0.85 Multiplicative Head Factor, and 0.5 Multiplicative Pressure Loss Factor

			Experiment 101201-1041 Cycle Points		
Measured Inlet Boundary Conditions	ω / RPM1 (kRPM)		25.00 (3397 s)	35.069 (4500 s)	39.14 (6100)
	$\dot{m}$ / FLOW (kg/s)		0.9734	1.631	1.630
	$T_{ti}\|_{corr}$ / T100 (C) (corrected)		146.3	146.5	202.0
	P_{ti} / P100 (MPa)		8.284	9.125	9.365
Outlet Conditions	T_{t1} / T200 (C)	Experiment	137.9	130.1	182.1
		Model	137.2	127.9	181.6
	P_{t1} / P200 (MPa)	Experiment	7.606	7.584	7.584
		Model	7.473	7.377	7.499
Validation Metrics	$\boldsymbol{\Delta P} = P_{t1} - P_{ti}$ (MPa)	Experiment	-0.6780	-1.541	-1.781
		Model	-0.8110	-1.748	-1.866
		Model Error	-0.133 (**20%**)	-0.207 (**13%**)	-0.085 (**5%**)
	$\boldsymbol{\Delta h}\|_{\boldsymbol{corr}}$ from $T_{ti}\|_{corr}$, P_{ti}, T_{t1}, and P_{t1} (kJ/kg)	Experiment	-6.449	-11.56	-16.12
		Model	-6.524	-13.05	-16.35
		Model Error	-0.075 (**1%**)	-1.490 (**13%**)	-0.230 (**1%**)

In conclusion reasonable agreement between the turbine model and the experiment data was achieved by introducing empirical correction factors f_{head} = 0.85 and f_{loss} = 0.5.

An independent comparison of the model is made using turbine state-point data given in [11] obtained there from Barber-Nichols turbomachine maps for the T-2 turbine design. Here is it assumed that in Figure 2.2 of [11] the state quantities given are in the pipe upstream and the pipe downstream of turbine. It is also assumed that the velocities in these pipes are small so that total and static pressure are essentially equal. Further, it is assumed that the dynamic head output from the impeller is converted to static head with 100 percent efficiency i.e. that the total pressures out of the impeller equals the static pressure in the pipe.

With the above assumptions, the present model is compared in Table 3.11against the data in Figure 2.2 of [11]. The table gives the present turbine predictions parameterized with respect to the multiplicative head factor, f_{head} , and the multiplicative pressure loss factor, f_{loss} . It is apparent that good agreement (shown in bold) is achieved with f_{head} = 0.85 and f_{loss} = 1.0.

Table 3.11 Comparison of Turbine Model State Points against those Derived from Barber-Nichols Model*

		Barber-Nichols Model [11]	Present Model		
			f_{head} = 1.0 f_{loss} = 1.0	f_{head} = 0.85 f_{loss} = 1.0	f_{head} = 0.85 f_{loss} = 0.5
Predicted Outlet Conditions	T_{t1} (^{0}C)	**476**	466	**479**	480
	P_{t1} (MPa)	**7.89**	6.98	**7.95**	8.41
	Δh (kJ/kg)	**68.0**	77.6	**64.0**	63.3
	η	**0.84**	0.80	**0.82**	0.90

*Boundary conditions: ω = 75 kRPM, T_{ti} = 537 ^{0}C , P_{ti} = 13.5 MPa , $\dot{m}$ = 2.58 kg/s

Future work might investigate the underlying causes that give rise to the need for these correction factors. First, a thermocouple mounted at the nozzle inlet would provide a better indication of temperature at this key point. Second, heat losses from the turbine could be measured directly. Allowing the impeller to free wheel at inlet conditions and measuring the temperature drop between inlet and outlet would provide a more accurate measure of heat loss. Finally, the enthalpy change during operation could be more accurately obtained by measuring the torque on the stator using strain gauges rather than by measuring pressure and temperature at inlet and outlet to infer thermodynamic states as done here. There is the possibility that the assumption in this work that the pressure and temperature measurements (from which enthalpy change is inferred) are total quantities is not born out in practice.

4 Summary and Recommendations

A one-dimensional model for a radial inflow turbine has been developed for super-critical carbon dioxide Brayton cycle applications. The model accounts for the main phenomena present in the volute, nozzle, and impeller of a single-stage turbine. These phenomena include internal losses due to friction, blade loading, and angle of incidence and parasitic losses due to windage and blade-housing leakage. The model has been added as a component in the G-PASS plant systems code.

The model was developed to support the analysis of S-CO_2 cycles in conjunction with small-scale loop experiments. Such loops operate at less than a MWt thermal input. Their size permits components to be reconfigured in new arrangements relatively easily and economically. However, the small thermal input combined with the properties of carbon dioxide lead to turbomachines with impeller diameters of only one to two inches. At these sizes the dominant phenomena differ from those in larger more typical machines. There is almost no treatment in the literature of turbomachines at these sizes. The present work therefore is aimed at developing turbomachine models that support the task of S-CO_2 cycle analysis using small-scale tests.

Model predictions were compared against data from an experiment performed for Sandia National Laboratories in the split-flow Brayton cycle loop currently located at Barber-Nichols Inc. The split-flow loop incorporates two turbo-alternator-compressor (TAC) units each incorporating a radial inflow turbine and a radial flow compressor on a common shaft. The

predicted thermodynamic conditions at the outlet of the turbine on the main compressor shaft were compared with measured values at different shaft speeds. Two modifications to the original model were needed to better match the experiment data. First, a representation of the heat loss from the volute downstream of the sensed inlet temperature was added. Second, an empirical multiplicative factor was applied to the Euler head and another to the head loss to bring the predicted outlet pressure into better agreement with the experiment. These changes also brought the overall efficiency of the turbine into agreement with values cited by Barber Nichols for small turbines.

More generally, the quality of measurement set data can in the future be improved by additional steps in the design and operation of the experimental apparatus. First, a thermocouple mounted at the nozzle inlet would provide a better indication of temperature at this key point. Second, heat losses from the turbine should be measured directly. Allowing the impeller to free wheel at inlet conditions and measuring the temperature drop between inlet and outlet would provide a more accurate measure of heat loss. Finally, the enthalpy change during operation is more accurately obtained by measuring the torque on the stator using strain gauges rather than by measuring pressure and temperature at inlet and outlet to infer thermodynamic states.

5 References

1. R. B. VILIM, “Development and Validation of G-PASS Compressor Model for Spilt-Flow Loop Simulation”, ANL-GenIV-144, August 2010.
2. R.H. AUNGIER, “Turbine Aerodynamics: Axial-Flow and Radial-Inflow Turbine Design and Analysis,” ASME Press, 2006.
3. W. JIANG, J. KHAN, and R.R. DOUGAL, Dynamic Centrifugal Compressor Model for System Simulation, Journal of Power Sources, 159, pp.1333-1343, 2006.
4. H.W. OH, E.S. YOON and M.K. CHUNG, An Optimum Set of Loss Models for the Performance Prediction of Centrifugal Compressors, Proceedings Institute of Mechanical Engineers, Vol. 211, Part A, pp. 331-338, 1997.
5. O. CONRAD, K. RAIF, M. WESSELS, The Calculation of Performance Maps for Centrifugal Compressors with Vane-Island Diffusers, ASME 25th Annual International Gas Turbine Conference, New Orleans, Louisiana, March 1980, pp. 135-147.
6. D.W. ARTT AND S.W. SPENCE, “A Loss Analysis Based on Experimental Data for a 99.0 mm Radial Inflow Nozzled Turbine with Different Stator Throat Areas,” Proceedings of the Institution of Mechanical Engineers, Part A: Journal of Power and Energy 1998 212: 27.
7. R.H. AUNGIER, “Centrifugal Compressors: A Strategy for Aerodynamic Design and Analysis,” ASME Press, 2000.
8. OERTEL, H., PRANDTL, L., and BOHLE, M., Prandtl’s Essential of Fluid Mechanics, Springer, Second Edition.
9. WRIGHT, S.A, *et al*, “Break-Even Power Transients for Two Simplified Recuperated S-CO_2 Brayton Cycle Test Configurations,” S-CO_2 Power Cycle Symposium, Boulder Colorado, May 2011.
10. S.A. WRIGHT, personal communication, Sandia National Laboratory, December 13,

2008.
11. WRIGHT, S.A, *et al*, "Gen-IV S-CO2 Brayton Cycle Test Loop Design and Split Flow S-CO2 Compressor Test Loop Construction Design," Sandia National Laboratories, September 15, 2008.

Appendix Theoretical Impeller Head

The torque exerted on impeller by unit mass of fluid is from Newton's Second Law

$$\boldsymbol{T} = \boldsymbol{r} \times \boldsymbol{F} = \boldsymbol{r} \times \frac{d}{dt}\boldsymbol{V} \tag{A.1}$$

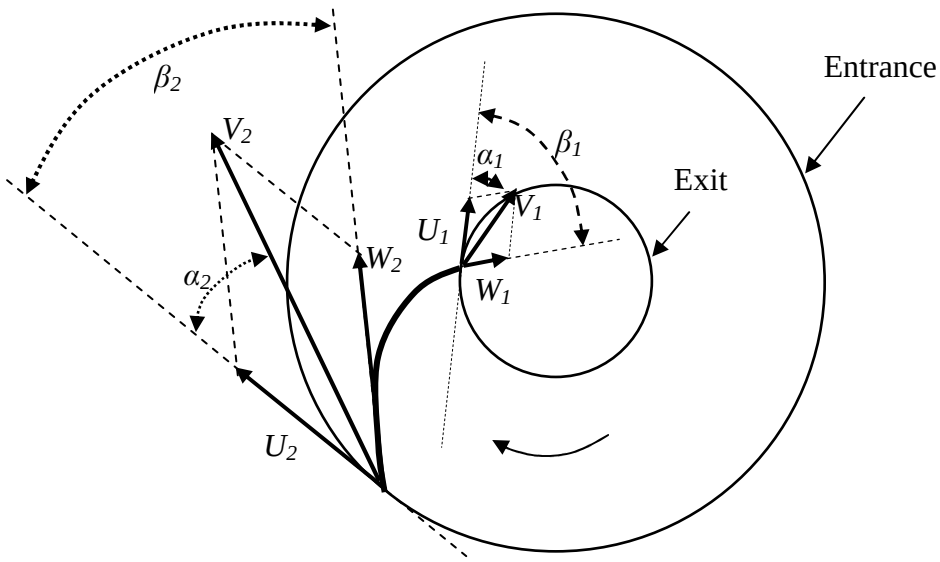

U	=	velocity of impeller edge
V	=	absolute velocity of fluid
W	=	velocity of fluid relative to impeller
	=	V - U
α	=	angle between V and U
β	=	blade angle

Figure A1. Diagram of Velocity Vectors at Entrance and Exit to Impeller

For the turbine impeller in Figure A.1 fluids enters at the outer radius of the impeller annulus and exits at the inner radius. Define a control volume whose surface coincides with these impeller radii. In the steady state it follows from Eq. (A.1) that the torque exerted on the impeller equals the net angular momentum change of the control volume so that:

$$T = \dot{m}\,(r_2 V_2 \cos\alpha_2 - r_1 V_1 \cos\alpha_1) \tag{A.2}$$

for a mass flow rate $\dot{m}$ through the turbine. The power imparted to the impeller by the control volume is then

$$\dot{Q} = T\omega = \dot{m}\,\omega\,(r_2 V_2 \cos\alpha_2 - r_1 V_1 \cos\alpha_1) \tag{A.3}$$

where ω is the angular speed of the impeller or from Figure A.1

$$\dot{Q} = \dot{m}\,(U_2 V_2 \cos\alpha_2 - U_1 V_1 \cos\alpha_1)\,. \tag{A.4}$$

The power is also given by

$$\dot{Q} = \dot{m}\,(h_2 + \tfrac{1}{2}V_2^{\,2} - h_1 - \tfrac{1}{2}V_1^{\,2}) \tag{A.5}$$

so that from the above two equations

$$H = U_2 V_2 \cos\alpha_2 - U_1 V_1 \cos\alpha_1 \tag{A.6}$$

or

$$H = U_2 V_{2\|} - U_1 V_{1\|} \tag{A.6}$$

where H is defined as the specific total enthalpy change

$$H = h_2 + \tfrac{1}{2}V_2^{\,2} - h_1 - \tfrac{1}{2}V_1^{\,2}\,. \tag{A.7}$$

The dependence of Eq. (A.6) on α and V is transformed into a dependence on turbine geometric parameters and angular speed. Now for i = 1 and 2

$$V_i \cos\alpha_i = U_i + W_i \cos\beta_i \quad \text{and} \tag{A.8a}$$

$$\frac{\dot{m}}{\rho_i} = 2\pi\, r_i\, b_i\, W_i \sin\beta_i \tag{A.8b}$$

where b_i is the height of the surface through which the fluid enters/exits the impeller.

Combining (A.8a) and (A.8b)

$$V_i \cos\alpha_i = U_i + \frac{\dot{m}}{2\pi\, r_i\, b_i\, \rho_i} \cot\beta_i\,. \tag{A.9}$$

Nuclear Engineering Division
Argonne National Laboratory
9700 South Case Avenue
Argonne, IL 60439

www.anl.gov

Argonne National Laboratory is a U.S. Department of Energy
laboratory managed by UChicago Argonne, LLC